

Chilean high-altitude hot-spring sinters: a model system for UV screening mechanisms by early Precambrian cyanobacteria

V. R. PHOENIX,^{1*} P. C. BENNETT,² A. S. ENGEL,³ S. W. TYLER⁴ AND F. G. FERRIS¹

¹*Department of Geology, University of Toronto, Ontario, Canada*

²*Department of Geological Sciences, The University of Texas-Austin, Austin, Texas, USA*

³*Department of Geology and Geophysics, Louisiana State University, Baton Rouge, Louisiana, USA*

⁴*Department of Geological Sciences and Engineering and Department of Natural Resources and Environmental Sciences, University of Nevada-Reno, Reno, Nevada, USA*

**Present address: Dept. Geographical and Earth Sciences, University of Glasgow, Gregory Building, Lilybank Gardens, Glasgow, UK*

ABSTRACT

Before the build-up of stratospheric ozone, Archean and early Proterozoic phototrophs existed in an environment subjected to highly elevated levels of ultraviolet (UV) radiation. Therefore, phototrophic life would have required a protective habitat that balanced UV attenuation and photosynthetically active radiation (PAR) transmission. Here we report on aspects of the phototroph geomicrobiology of El Tatio geothermal field, located at 4300 m in the Andes Mountains of northern Chile (22 °S), as an analogue system to early Precambrian environments. El Tatio microbes survive in a geochemical environment of rapidly precipitating amorphous silica (sinter) and unusually high solar radiation (including elevated UV-B flux) due to the high-altitude, low-latitude location. Cyanobacteria produce 10-mm-thick surface mats containing filaments encased in amorphous silica matrices up to 5 µm thick. Relative radiation absorbance of these silica matrices was UV-C > UV-B > UV-A > PAR, suggesting the silica provides a significant UV shield to the cyanobacteria. Cyanobacteria also occur in cryptoendolithic communities 1–10 mm below siliceous sinter surfaces, and in siliceous stromatolites, where viable cyanobacteria are found at least ~10 mm below the sinter surface. UV-B was dramatically attenuated within ~1 mm of the sinter surface, whereas UV-C (a frequency range absent today but present in the early Precambrian) was attenuated even more efficiently. PAR was attenuated the least, and minimum PAR levels required for photosynthesis penetrated 5–10 mm into the sinter. Thus, a favourable niche occurs between approximately 1–10 mm in siliceous sinters where there is a balance between PAR transmission and UV attenuation. These deposits also would have strongly attenuated Archean and early Precambrian levels of UV and thus, by analogy, cyanobacteria of early Precambrian shallow aquatic environments, inhabiting silicified biofilms and silica stromatolites, would have similarly been afforded protection against high-intensity UV radiation.

Received 30 May 2005; accepted 10 January 2006

Corresponding author: V. R. Phoenix. Tel.: +44 (0)141 330 5474; fax: +44 (0)141 330 4894; e-mail: v.phoenix@ges.gla.ac.uk.

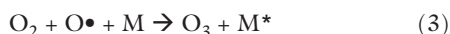
INTRODUCTION

The proliferation of oxygenic phototrophs in the early Precambrian initiated the increase in atmospheric oxygen (O₂), beginning approximately 2.5 Ga. Problematically, since ozone is derived from photochemical reaction of oxygen in the upper atmosphere, the earliest period of photosynthesis would have occurred prior to the build-up of sufficient ozone to attenuate ultraviolet (UV) radiation. Precambrian phototrophs would therefore require a suitable mechanism to attenuate harmful UV wavelengths while still allowing transmittance of sufficient photosynthetically active radiation (PAR, 400–700 nm) for

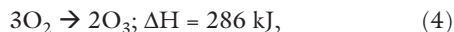
effective photosynthesis. We report here a field example of a UV-protective habitat, defined by an association between a phototrophic community and a porous siliceous material that balances UV attenuation and PAR transmittance. This environment may be an analogue of early Precambrian habitats where primitive phototrophs evolved, protected from damaging UV radiation.

Ozone is produced in the upper stratosphere via the Chapman Cycle, whereby short wavelength UV (<242 nm) radiation (*hν*) reacts with molecular O₂ to produce ozone (O₃):

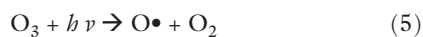




where $\text{O}\bullet$ is an oxygen free radical, and M is any other molecule, typically either N_2 or O_2 . The net reaction is



which at high partial pressures of molecular O_2 establishes a highly absorbing stratospheric O_3 layer. The photochemical reaction that attenuates the longer wavelength UV ($<300 \text{ nm}$; $\lambda_{\text{max}} = 250 \text{ nm}$) radiation is



and scant solar radiation with wavelengths shorter than 290 nm penetrates the present-day atmosphere (Caldwell *et al.*, 1989).

UV-B ($280\text{--}320 \text{ nm}$) and, in particular, UV-C ($200\text{--}280 \text{ nm}$) are damaging and ultimately lethal to life at a wide range of frequencies, although UV radiation is most harmful at wavelengths between 240 and 270 nm due to strong absorption of light at these frequencies by DNA (see review by Tevini, 1993). UV radiation can also damage cellular processes through inhibition of protein synthesis (Jeffery *et al.*, 1996) and deactivation of enzymes (Tevini, 1993). In cyanobacteria, the reaction centre of photosystem II is damaged, resulting in photo-inhibition (Hader & Worrest, 1991). Overexposure to UV can also result in bleaching of photosynthetic pigments and reduction in cyanobacterial motility (Donkor & Hader, 1991).

During much of the Archean, geochemical evidence suggests that levels of atmospheric O_2 were low, possibly as low as 10^{-13} of the present atmospheric level (PAL) (Kasting, 1987). This exceedingly low partial pressure of O_2 would produce negligible concentrations of O_3 by the Chapman Cycle, allowing the transmission of very high levels of biologically detrimental UV-C and UV-B radiation to the Earth's surface, even with the predicted lower solar luminosity (Berkner & Marshall, 1965; Walker *et al.*, 1983; Kasting, 1987; Pierson *et al.*, 1993). Somewhat understandably, there is no single consensus on the composition of the Archean atmosphere. Several models predict atmospheric compositions which adsorb greater levels of UV (see Cockell, 2002 for summary). In this study, however, we consider the implications of the low absorption, high UV flux, scenario.

At the end of the Archean (2.5 Ga) geochemical evidence suggests that the partial pressure of O_2 began to increase, reaching $\sim 10^{-3}$ PAL at 2.0 Ga , and rising steadily thereafter (Walker *et al.*, 1983; Kasting, 1987). Although O_2 partial pressures of 10^{-3} PAL would have supported some O_3 production that would attenuate a proportion of incident UV-C and UV-B, damaging fluxes still would have been transmitted to the Earth's surface (Cockell, 2000).

During the early Precambrian, photosynthesizing microorganisms inhabiting deeper marine environments may have

been protected from UV by the water column, providing they lived at a specific depth range that also transmitted sufficient PAR (Sagan, 1973; Margulis *et al.*, 1976; Olson, 1981; Cockell, 2000). Recent studies suggest that 30 m of ocean water would have been required to reduce UV damage to the same levels experienced on the surface today (Cockell, 2000). The geological record, however, reveals many Archean and early Proterozoic cyanobacterial communities existed in shallow-water environments, some repeatedly subaerially exposed, that would have been subjected to intense UV irradiation (e.g. Cloud, 1965; Awramik *et al.*, 1983; Lowe, 1983; Walter, 1983; El Tabakh *et al.*, 1998; Hofmann *et al.*, 1999). In these shallow marine environments or in subaerially exposed settings, cyanobacteria may have utilized UV screening mechanisms such as matting habit (Rambler & Margulis, 1980), phototaxis (Margulis *et al.*, 1976), sheath pigmentation (Garcia-Pichel & Castenholz, 1991) and photo repair mechanisms (Walter, 1983). Although these mechanisms are effective, cells and cellular processes may still be damaged and eventually made ineffective by UV radiation, thus more robust UV screening mechanisms would have offered a substantial advantage prior to the development of an effective O_3 shield. Pierson *et al.* (1993) described how burial under thin layers of sediment, such as iron enriched amorphous silica, sands and calcite, would have provided an effective UV screen and Phoenix *et al.* (2001) demonstrated in a laboratory study how amorphous-silica biomineralization of cyanobacteria could provide an effective UV screen.

Silica precipitation and biomineralization were a characteristic of the Archean and early Proterozoic marine environment and were important in the formation of many siliceous cherts, stromatolites and the preservation of microfossils (Cloud, 1965; Lowe, 1983; Holland, 1984; Sugitani, 1992). At that time, marine waters contained high concentrations of dissolved silica (Cloud, 1965; Holland, 1984; Siever, 1992; Sugitani, 1992) and this, combined with the impact of evaporation in such shallow intermittently exposed settings drove silica precipitation (Holland, 1984). While the precipitation of amorphous silica was abundant in these ancient marine settings, the precipitation of carbonates and evaporate minerals was also abundant (Dunlop *et al.*, 1978; Lowe, 1980, 1983), although the UV screening properties of these precipitates are not considered here.

Today, silica-enriched hot-spring settings provide an analogue for ancient microbial habitats, and studying these modern environments and their associated sinters (silica precipitates) provide insights into microfossil preservation and siliceous stromatolite formation in the Precambrian (e.g. Walter, 1972; Schultze-Lam *et al.*, 1995; Cady & Farmer, 1996; Jones *et al.*, 1998; Konhauser *et al.*, 2001). Although the potential for silicification to act as a UV shield has been demonstrated in the laboratory (Phoenix *et al.*, 2001), this mechanism has yet to be evaluated in a natural, high UV flux setting. Phoenix *et al.* (2001) only examined the UV shielding characteristics of a silicified biofilm of a single species in a simple laboratory

setting, while this field study investigates UV shielding in complex natural communities and furthermore, allows characterization of UV shielding in cryptoendolithic and stromatolitic communities. In addition, the current study considers the impact of the full solar spectrum between UV-C and PAR for both contemporary and ancient communities. This contrasts the Phoenix *et al.* (2001) study which only considered the impact of UV-C.

The modern El Tatio geothermal field in northern Chile provides a particularly suitable locality for such a study. Here silica-rich hot-spring waters discharge near local boiling temperature in geyser complexes, and thick terraces of hydrous amorphous and opaline silica precipitates are associated with the geysers. El Tatio is a hyperarid, high-elevation (~4300 m) location, with UV-A and UV-B flux approximately 35% greater than at a high-humidity, sea-level setting (Piazena, 1996).

Geological and hydrogeological setting

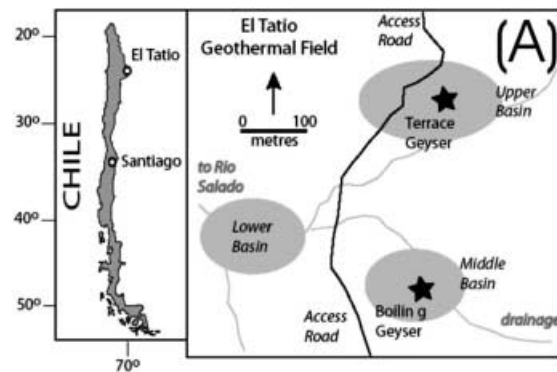
The geothermal field at El Tatio is located near the Chile–Bolivia border in the northern Antofagasta Province (II Region) of Chile (Fig. 1A), at the northern edge of the Atacama Desert region. The basin is geologically associated with the Altiplano–Puna Volcanic Complex, in the north–south trending Tatio Graben, bounded on the east by the Serrania de Tucle-Loma Lucero horst and on the west by El Tatio volcanics (Lahsen & Trujillo, 1976; de Silva & Francis, 1991). The geothermal field is ~30 km², but surface thermal features are found within 10 km² in three distinct basins (Upper, Middle, and Lower basin) (Fig. 1A). A detailed physiographic description of the basin can be found in Glennon & Pfaff (2003) with each hydrothermal feature identified and described.

Most of the hot-springs discharge near local boiling temperature (~86 °C). Siliceous sinter deposits are found throughout the geothermal field, sometimes as large cones at geyser vents or as terraces at the geysers and springs (Fig. 1B,C). The source of the hot-spring water is snowmelt from the nearby Andes Mountains, with the thermal source water entering the basin from the south-east with a maximum measured subsurface temperature of 212 °C at 400 m in test hole no. 5 (Mahon, 1971). The silica and Na/K geothermometers provide a calculated maximum subsurface temperature of 222–224 °C (Giggenbach, 1978; Fournier & Potter, 1982).

MATERIALS AND METHODS

Discharge water, sinter and biomass were sampled throughout the geothermal field during a field campaign in January

Fig. 1 (A) Location map of El Tatio, northern Chile. Modified from Glennon & Pfaff (2003). (B) Terrace geyser of the Upper Basin around which the sampling was focused (showing 3-m-high eruption and discharge apron). (C) 1-m-high terrace of same geyser showing discharge apron and cyanobacterial mat draped over the sinter surface (CM).



2003. For this report, however, we discuss in detail the Terrace Geyser, a feature in the Upper Basin with a gently sloping, multitiered 1-m-high sinter terrace and thick cyanobacterial mats (Fig. 1B,C). All results are from the Terrace Geyser location, unless otherwise stated (e.g. bulk geochemical data from all three basins are presented, and some data are presented from a geyser feature in the Middle Basin, referred to here as the Boiling Geyser). Throughout the field investigations, the Terrace Geyser perpetually spouted to a height of 2–3 m above the terrace surface; Glennon & Pfaff (2003) reported that this feature can be more geyser-like and intermittently erupts at 30 min to 2 h intervals to a height of 5 m. Water flowed away along a broad discharge apron, and siliceous oncoids associated with this feature were studied by Jones & Renaut (1997). In comparison, the Boiling Geyser erupted every minute as a frothy fountain to a maximum observed height of 1 m above a static water level. At both sites, depending on wind direction, water sprayed the surrounding sinter surfaces. Wetted sinter surfaces would often undergo periods of drying due to the combined effects of intense solar radiation and low humidity. Further details of El Tatio sinter architecture and formation are provided by Jones & Renaut (1997) and Fernandez-Turiel *et al.* (2005).

Biomass characterization

(Cyano)bacterial samples were collected both from the sinter surfaces and from microbial layers inside the sinter, up to 10 mm below the surface (details of the microbial communities and layering are discussed later in the results). Duplicate samples were collected and stored in sterile plastic 1.5 mL tubes; one set was kept for culturing (no additional solutions were added to the storage tubes) and 2.5% glutaraldehyde was added to the second set as a fixative for electron microscopy. Conservative samples of silica sinter were carefully broken free and placed in sterile whirl-pak bags to prevent dehydration.

On return to the laboratory, cyanobacterial cultures from the microbial mats and from within sinter samples were grown on agar plates and in liquid media using both BG11 –N and BG11 +N nutrients (Rippka *et al.*, 1979) at 28 °C under cool white fluorescent lamps (24 $\mu\text{mol m}^{-2} \text{s}^{-1}$). Additionally, cyanobacteria were collected from within the sinter and their viability was appraised using phycoerythrin autofluorescence (this phycobilin is dispersed upon lysis) using a Nikon Microphot-FXA fluorescence microscope (Nikon Canada Inc., Mississauga, Canada). Phycoerythrin autofluorescence was used as an indicator of viability as this natural autofluorescence makes the use of traditional viability stains problematic. To prevent confusion from weak autofluorescence due to lingering phycoerythrin after cell death, we only considered strongly autofluorescing cells as viable candidates. This, combined with culturing, enabled an appraisal of cell viability within the sinters. Identification of cyanobacteria to the genus level was performed using light microscopy, using the taxonomic scheme

of Rippka *et al.* (1979). The large size of these organisms facilitated this approach. Visual identification forms the basis of this popular taxonomic scheme and hence this approach was deemed appropriate considering the scope of the study. The goals of this study do not include community analysis by more advanced molecular methods.

Mat samples fixed in glutaraldehyde were processed for transmission electron microscopy (TEM) as described in Phoenix *et al.* (2000). TEM was performed on a Leo 912AB operating at 100 Kv. Polished petrological thin sections were made from the siliceous sinter and examined on a Leitz Wetzlar petrological microscope. Digital images were collected using a 3CCD Donpisha colour vision camera and SCION IMAGE software (Scion, Frederick, MD, USA).

Water and sinter geochemistry

Water samples were collected at a total of 30 geyser features and from locations along geyser outflow channels. Samples were analysed for transient parameters (pH, ORP) at ambient temperatures immediately in the field using electrodes stable at those temperatures. Samples were filtered in the field to 0.1 μm and preserved for metal and metal speciation analysis. Water samples were analysed in the laboratory for anions by single column ion chromatography, metals by ICP-MS, and carbon species by carbon analyser. Arsenic redox speciation was determined using the SPE method of McCleskey *et al.* (2004) on a filtered sample preserved with EDTA with analysis by ICP-MS. Solute speciation and saturation state with respect to mineral phases was calculated using the geochemical model PhreeqC (Parkhurst & Appelo, 1999).

Sinter samples collected for geochemical analysis were characterized by electron microprobe on polished thick sections using a JEOL 8200, and additionally by laser ablation (LA) ICP-MS (Micromass Platform). Samples of freshly fractured siliceous sinter and associated biomass were examined using a FEI-Philips XL-30 environmental scanning electron microscope (ESEM) (FEI, Hillsboro, OR, USA), with gaseous secondary and backscatter electron detectors and qualitative elemental analysis by X-ray energy dispersive spectrometer. Chamber conditions for observations were varied from 10–95% relative humidity using a peltier cooling stage and variable H_2O partial pressure.

Fresh siliceous precipitates were also collected on transparent artificial substrata in the field. One-millimetre-thick glass slides and polyolefin film were placed in the outflow channels and discharge aprons of the Terrace and Boiling Geysers (Fig. 1) to collect precipitate. The fresh precipitates were examined by ESEM and LA-ICP-MS.

Field and laboratory radiation measurements

Solar radiation measurements of bulk PAR (400–700 nm), UV-A (320–400 nm) and UV-B (280–320 nm) were measured

in-field using a Macam Photometrics Q203 PAR meter (Macam Photometrics Ltd, Livingston, UK) with PAR Cos-112 quantum response filter ring for measuring PAR, and a Macam Photometrics UV203 meter with a UVA – Cos filter ring for measuring UV-A and a UVB2 – Cos filter ring for measuring UV-B. The detectors contain a light input diffuser which allows detection of photons arriving at angles up to at least $\pm 70^\circ$ about the zenith, enabling effective measurement of down welling scattered and direct light. The UV203 meter with UVB2 filter ring has a peak response at 311 nm, with a full half bandwidth (i.e. bandwidth at half maximum relative response) of 303 nm to 321 nm. The UV203 meter with UVA filter ring has a peak response of 365 nm and full half bandwidth of 345 nm to 379 nm. The specific analysis of solar radiation was supplemented with larger scale measurements of local meteorological parameters: temperature, wind direction, relative humidity and heat flux recorded on a Campbell Scientific data logger.

Light transmission was measured in the laboratory on sinter samples and fresh precipitates. Sinter was sectioned in the laboratory into wafers 1.4–10 mm in thickness (thinner sections could not be cut as this resulted in disintegration of the sinter). Absorption of PAR, UV-A, UV-B, and UV-C by the sinter wafers was measured using light from Cole-Palmer 9815 series lamps (Cole-Palmer Canada Inc., Anjou, Canada) at 15 cm (UV-A = 6.1 Wm^{-2} ; UV-B = 6.8 Wm^{-2} ; or UV-C = 4.0 Wm^{-2}). A 60 W tungsten/22 W cool white combination lamp was used as the PAR source. Measurements were taken through a fixed wafer area using the UV203 and Q203 radiometers, as described above. For measuring UV-C, an IF-254 filter ring was used with the UV203 radiometer (peak response at 254.5 nm and full half bandwidth of 250 nm to 261.5 nm). Light transmission was also measured on sinter samples saturated with a 5 mM SiO_2 solution. This was done to test how the difference in refractive index between a sinter-air and sinter-hydrothermal fluid system would impact irradiance attenuation. Absorption measurements of the fresh precipitates collected on glass slides and plastic film were measured as described above, and using a PerkinElmer Lambda 6 UV/VIS spectrophotometer (PerkinElmer, Boston, MA, USA) scanning from 200 to 700 nm at 1-nm resolution to collect continuous spectra. To compensate for substratum effects, UV/VIS absorption by glass slides and plastic film alone were measured. Thus precipitate absorption was determined as the difference between the total absorption (substratum plus the precipitate) and the substratum alone.

RESULTS

Water and sinter geochemistry

Representative water analyses from the three basins are summarized in Table 1. Geyser waters are circumneutral to slightly alkaline pH (neutral pH is 6.26 at 85 °C), Na-Cl-type waters, and moderately saline with unusually high concentrations of Cs, Li, and Rb. Conservative solutes increased along the discharge channels, indicating rapid evaporation in the extremely dry atmosphere. Total dissolved inorganic carbon concentrations were low, and were calculated to be in approximate equilibrium with atmospheric Pco_2 . The waters have exceptionally high concentrations of both As and Sb (Table 1), higher than virtually any other hot-spring water presently known, with As speciated predominately as the more toxic As(III).

Geyser waters at the upper basin discharge with 145–160 p.p.m. dissolved Si (Table 1). At the average discharge temperature the waters are in approximate equilibrium or slightly undersaturated with respect to amorphous silica, and supersaturated with respect to other polymorphs of silica (e.g. Iler, 1979; Fournier & Potter, 1982). The silica equilibrium temperature of the Terrace Geyser waters (the temperature below which the waters would be supersaturated with respect to that phase) was determined to be 82 °C. The rapid cooling of the discharge water, coupled to intense evaporation in the dry air at El Tatio results in the system quickly becoming supersaturated with respect to amorphous silica; silica concentrations decrease along the outflow channels indicating silica precipitation. Silica also precipitates between outflow channels due to evaporation of geyser spray.

Desiccated sinter between the discharge channels at the Terrace Geyser contained distinct hydrated opal types that could be discriminated from each other in transmitted light and electron microscopy. Clear opal displayed large variations in hydration state and manifested varve-like zones at the micron scale. Less-translucent, inclusion-rich opal filled interstices between clear opal, and was uniformly dehydrated, but did not display the extremely regular laminations seen in the clear opal. Inclusion-rich opal also contained abundant voids consistent with morphologies and sizes of mineralized microbial filaments. In addition to Si, the sinter was composed of Sb, Ca, and Na; Sb ranged from ~0.5% (wt/wt as Sb_2O_5) to 3.5%. Only trace As was found in the silica sinter, although the concentration in the discharge water was very high. Laminated, clear opal had

Table 1 Representative water analyses. Concentrations are in millimolal

Basin	T (°C)	pH	[Cl]	[Na]	[Ca]	[Si]	[As]	[Sb]	[K]	[Li]	DIC
Middle	80.8	7.0	163	132	7.1	4.22	0.45	0.021	4.58	4.0	0.39
Upper	86	6.9	199	175	6.4	5.17	0.52	0.034	14.2	5.5	0.14
Lower	78	7.4	155	157	6.0	3.13	0.35	0.020	5.6	4.0	0.88

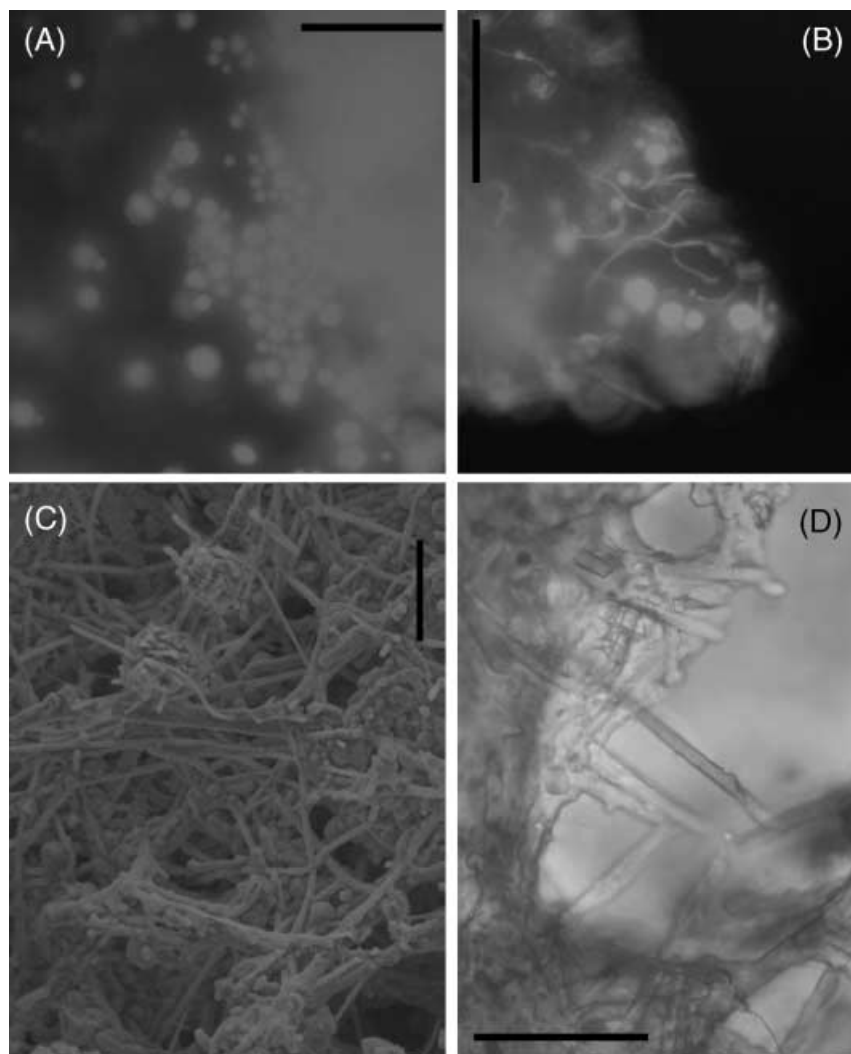


Fig. 2 Black and white autofluorescence micrograph of cryptoendolithic cells in silica sinter. (A) *Chroococidiopsis* spp. and (B) *Phormidium* spp. (thin filaments) and *Chroococidiopsis* spp. cells. The viable cells strongly fluoresce red (shown in white in this B & W image) indicating the presence of the pigment phycoerythrin, suggesting the cells are likely viable. Bright undefined areas in images are due to fluorescence of cells buried deeper into the sinter particle; the light leaving these is blurred due to scattering effects. Samples were taken from 10 mm below the sinter surface. Scale bars = 50 μm . (C) Environmental scanning electron micrograph of cryptoendolithic cyanobacteria (filaments and rods) in a pore space in silica sinter. Scale bar: 25 μm . (D) Petrographic light micrograph (thin section) of *Phormidium* spp. filaments in a pore space in silica sinter. Scale bar: 40 μm .

highly variable Sb and Ca concentrations, and these elements are generally more abundant within the more hydrated zones. The relatively dehydrated inclusion-rich opal, however, contained uniformly low concentrations of Sb and Ca.

Approximately 2- μm -thick fresh hydrous amorphous silica precipitates accumulated on artificial substrata after only four days of exposure to the geyser waters. The silica could be effectively sampled by electron microprobe and by LA-ICP-MS on the glass slides, and were found to be somewhat heterogeneous, with rare regions of compositional variability visible in BSE imaging (data not shown). The elemental analysis showed that the silica precipitates contained up to 12 wt percentage Ca, <6% K and <2% Sb (oxygen not included in these analyses).

Cyanobacterial communities – cryptoendoliths

The geothermal field at El Tatio initially appears barren of photosynthetic life (i.e. no cyanobacteria or higher plants), except for thick (up to 10 mm) cyanobacterial biofilms in some

of the discharge aprons, outflow channels and spray inundated areas. However, examination of the ‘barren’ sinter between the hot-springs in the Terrace Geyser area revealed deep-green cyanobacterial communities living within the sinter, 1–10 mm below the surface. Light microscopy of these communities revealed they were composed of spherical, unicellular cyanobacteria (~5–10 μm in diameter) morphologically consistent with *Chroococidiopsis* spp., and thin (~1 μm in diameter) filamentous cyanobacteria with either cylindrical or tangential disc-shaped cells, morphologically consistent with *Phormidium* spp. (those with tangential disc shaped cells could be *Phormidium* spp. or another LPP type). These three organisms were successfully cultured from material taken from 10 mm below the surface, indicating at least some cells were viable. This was corroborated by phycoerythrin autofluorescence analysis, which showed that >95% of the *Chroococidiopsis* spp. cells from below the surface (10 mm depth) exhibited strong autofluorescence consistent with viable cells (Fig. 2A). Phycoerythrin autofluorescence counts of *Phormidium* spp. were difficult, as the very thin filaments were often obscured by larger silica granules

(therefore dead, nonfluorescing filaments could not be counted easily). However, an abundance of strongly fluorescing filaments indicated that many were viable at depth (up to 10 mm) (Fig. 2B). Further examination of the sinter by ESEM and light microscopy revealed structures consistent with predominately filamentous microbial cells, which lacked a preferred alignment, grew cryptoendolithically and occupied voids and cavities within the sinter (Fig. 2C,D).

Cyanobacterial communities – stromatolites

Sinter samples collected from the outflow channel of the Terrace Geyser were stromatolitic in nature (i.e. containing alternating microbial and microbe free layers). Thicknesses of each lamina varied, ranging from 1 to 10 mm. Light microscopy revealed the microbial layers were dominated by large diameter (10–15 μm) cyanobacterial filaments encrusted in amorphous silica. These exhibited disc-shaped tangential cells and thick sheaths and were identified as *Lyngbya* spp. The genera *Calothrix* spp. (ensheathed, tapering filaments with terminal heterocysts) and *Phormidium* spp. were also present. Filaments commonly exhibited a random orientation, but in places a distinct horizontal alignment was observed.

Successful culturing from a cyanobacterial layer 10 mm below the surface indicated the presence of viable cells, yet phycoerythrin autofluorescence suggested that only 5–10% of cells were still viable at this depth. This could have been due, in part, to the preservation of sheaths and other cellular material by silicification which notably increased the apparent ‘dead’ biomass of the community. Further evidence of cell viability at depth within the stromatolite was observed at the Terrace Geyser after collection of the sinter; sampling re-exposed the subsurface microbial layers to sunlight and spring water. After two days re-exposure, the microbial layers had changed from brown to green in colour, suggesting production of chlorophyll-a and rejuvenation of the cyanobacterial colonies.

Cyanobacterial communities – surface biofilms

The thick (~10 mm) cyanobacterial mat on the surface of the stromatolite within the discharge apron exhibited the same general cyanobacterial composition as the layers below and was again dominated by *Lyngbya* spp. TEM analysis revealed that the surface cyanobacterial filaments were encrusted with amorphous silica colloids; the colloids approximately 30–400 nm in diameter. The colloids occurred predominantly on the outer surface of the thick fibrous sheath and formed colloidal crusts up to 5 μm thick (Fig. 3). *Anabaena* spp. were also identified in the surface biofilm.

Light intensity and attenuation

Solar zenith at El Tatio during the field period produced a maximum total solar radiation of 1206 W m^{-2} , while PAR

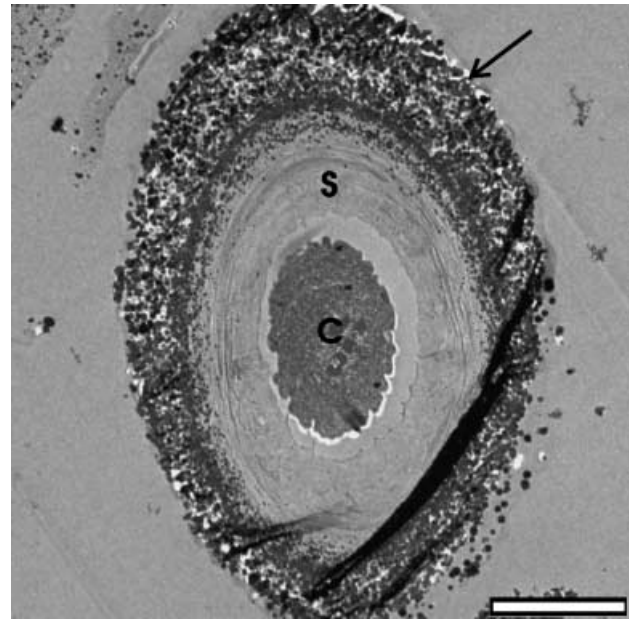


Fig. 3 TEM micrograph of a cyanobacterial cell encrusted in silica colloids. C = cell; S = polysaccharide sheath; arrow = layer of colloidal amorphous silica. Scale bar: 5 μm .

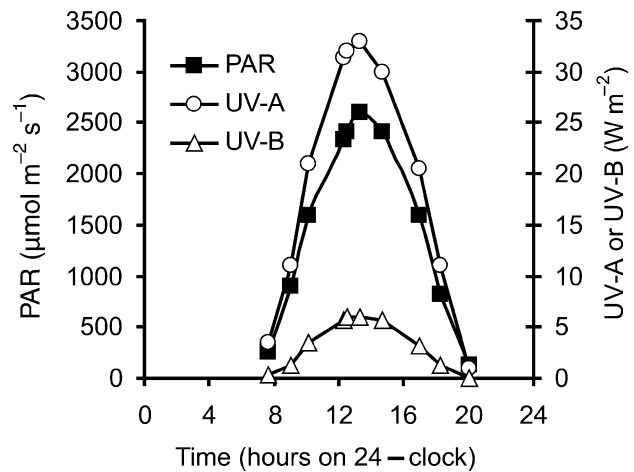


Fig. 4 Radiation profile for El Tatio on January 5, 2003, showing PAR, UV-A and UV-B intensities. See methods section for specification of radiometers used.

peaked at 2600 $\mu\text{mol m}^{-2} \text{s}^{-1}$. UV-A was 33.0 W m^{-2} and UV-B was 6.0 W m^{-2} (Fig. 4). Repeated measurements over several days produced consistent readings.

Radiation absorption analysis from the 2- μm -thick hydrous amorphous silica precipitates collected on glass slides and plastic films revealed the greatest attenuation of UV-C, followed by UV-B, UV-A, and PAR (Fig. 5A). Average absorbance values (and their standard deviations; $n = 8$; $\sigma = 1$) were 13.3% ($\pm 5.2\%$) for PAR, 21.2% ($\pm 8.7\%$) for UV-A, 29.0% ($\pm 10.8\%$) for UV-B and 66.3% ($\pm 11.0\%$) for UV-C. The continuous

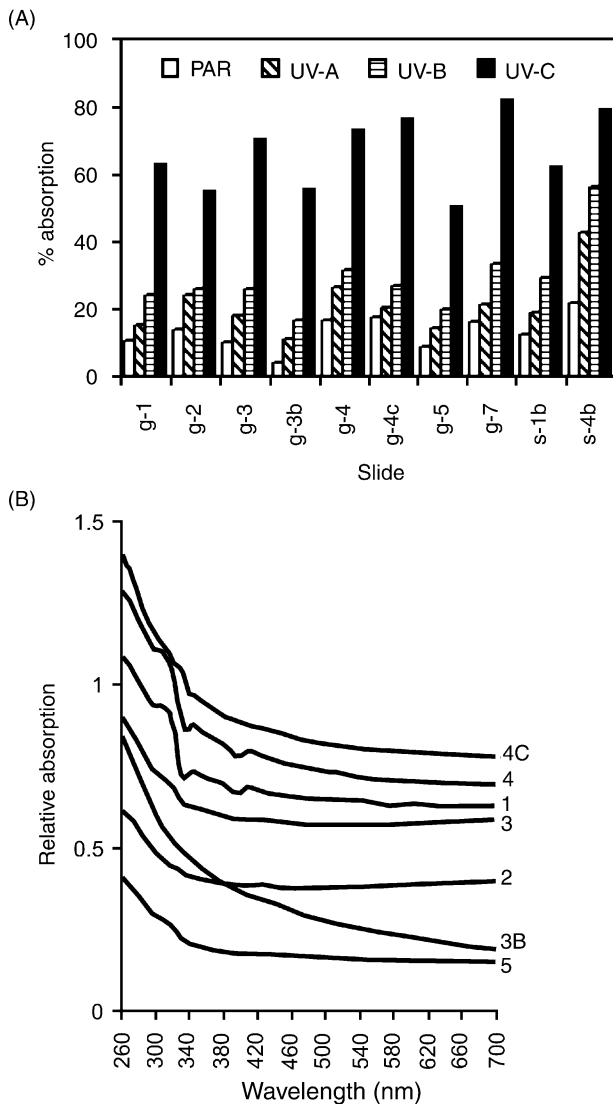


Fig. 5 (A) % absorption of PAR, UV-A, UV-B and UV-C by siliceous precipitates ($\sim 2 \mu\text{m}$ thick) collected on glass slides or thin plastic left in the discharge apron and outflow channels of the Terrace Geyser (except 1, 2 and 1b, which are from the Boiling Spring in Middle Basin). Samples labelled with the prefix 'g' were precipitates collected on glass slides and those with the prefix 's' were precipitates collected on plastic film. Data collected using a Macam radiometer. (B) Continuous absorption spectra of silica precipitates collected on glass slides. Data collected using a spectrophotometer. Labels correspond to glass slides in (A).

absorption spectra collected by UV/VIS spectrophotometer also showed the greatest absorption of shorter wavelengths by the precipitates (Fig. 5B), consistent with the absorption spectra of amorphous silica.

Sinter samples also attenuated UV radiation in the order UV-C > UV-B > UV-A > PAR (Fig. 6). Even the thinnest (1.4 mm) sinter wafers showed significant absorption of the most damaging wavelengths, absorbing 93–99% UV-B and 97–100% UV-C. In contrast, PAR attenuation was significantly less (e.g. the 1.4 mm wafers absorbed 78–92%), and this

waveband was able to penetrate deeper into the sinter (Fig. 6). When light attenuation was measured on 'wet' sinters (i.e. those saturated with 5 mM SiO_2 solution), transmittance was only slightly increased (Fig. 7; for brevity, results are shown just for sinter 'a', although all three sinter types showed similar small increases in transmittance due to wetting). The small increase in transmittance by wet sinters was, in general, proportional to the transmittance of the dry sample, such that the greatest increases were observed for PAR and the smallest for UV-C. These findings are consistent with previous studies showing increased transmittance in wet sand compared to dry sand (Kuhl & Jorgensen, 1994).

DISCUSSION

Although UV radiation varies greatly with location, incident solar UV radiation reaching the Earth's surface today is greatly attenuated by stratospheric O_3 and other gases. Despite this, the levels of UV-B that penetrate the ozone screen can still be damaging to cyanobacteria (e.g. Walsby, 1968; Donkor & Hader, 1991; Quesada & Vincent, 1997). The problem of UV damage is much greater at El Tatio; a high-altitude, low-latitude, low-humidity environment where midday UV-B intensity can exceed 6 W m^{-2} . For comparison, at Yellowstone National park, Wyoming (USA), maximum UV-B intensity at Octopus Spring (elevation <3000 m) is less than 4 W m^{-2} (Miller *et al.*, 1998).

Previous studies have demonstrated that cyanobacteria can suffer significant damage within 1 h of exposure to UV-B at 4 W m^{-2} (Hader *et al.*, 1986), an intensity that is equalled or exceeded at El Tatio at least 6 h each day during the austral summer (Fig. 4). Quesada & Vincent (1997) demonstrated that *Phormidium* (a genus also isolated from El Tatio during this study), maintained positive growth only when UV-B levels were less than 1 W m^{-2} . However, our sinter attenuation results demonstrate that the maximum midday UV-B radiation at El Tatio is reduced to less than 1 W m^{-2} (i.e. >83% attenuation) under $\sim 1 \text{ mm}$ of silica sinter (Fig. 6). Of course, different cyanobacterial groups will exhibit different UV-B tolerances, and some will exhibit significantly greater UV resistance (e.g. Dillon *et al.*, 2003). However, UV attenuation by the sinter is considerable, and it is clear that the viable cryptoendolithic and stromatolitic communities found 1–10 mm below the sinter surface were afforded considerable UV-B protection by the silica sinter, irrespective of each cyanobacterial strains own inherent UV resistance.

Attenuation of PAR by the sinter is also important to consider. Cyanobacteria commonly exhibit PAR saturation values (the PAR intensity at which maximum photosynthetic activity occurs) between 50 and $500 \mu\text{mol m}^{-2} \text{ s}^{-1}$ (Paerl *et al.*, 1985; Ibelings & Maberly, 1998; Hu *et al.*, 2000; Litchman, 2000; Litchman *et al.*, 2003). This is considerably less than the PAR incident at the sinter surface for much of the day at El Tatio (Fig. 4). PAR levels greater than saturation can be detrimental to cyanobacteria, inducing photoinhibition (Paerl *et al.*, 1985;

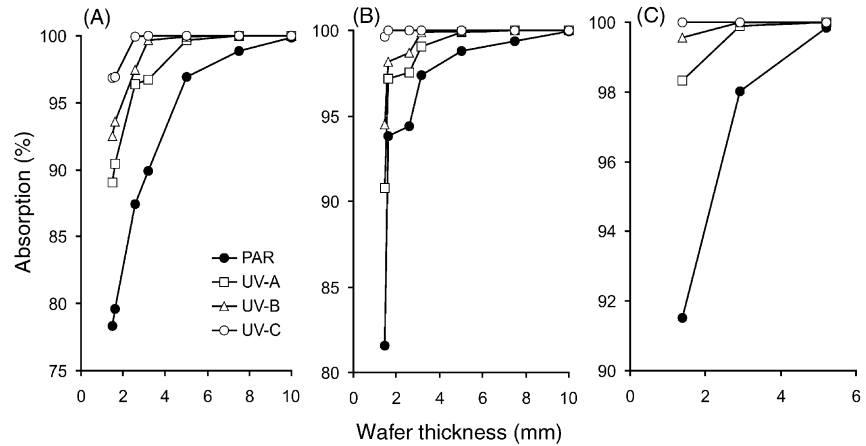


Fig. 6 % absorption of PAR, UV-A, UV-B and UV-C by wafers of silica sinter. Samples (A), (B) and (C) are different types of sinter. (A) Milky white sinter dominated by clear opal. (B) Grey sinter dominated by less translucent inclusion rich opal. (C) Sinter composed of cemented silica ooides.

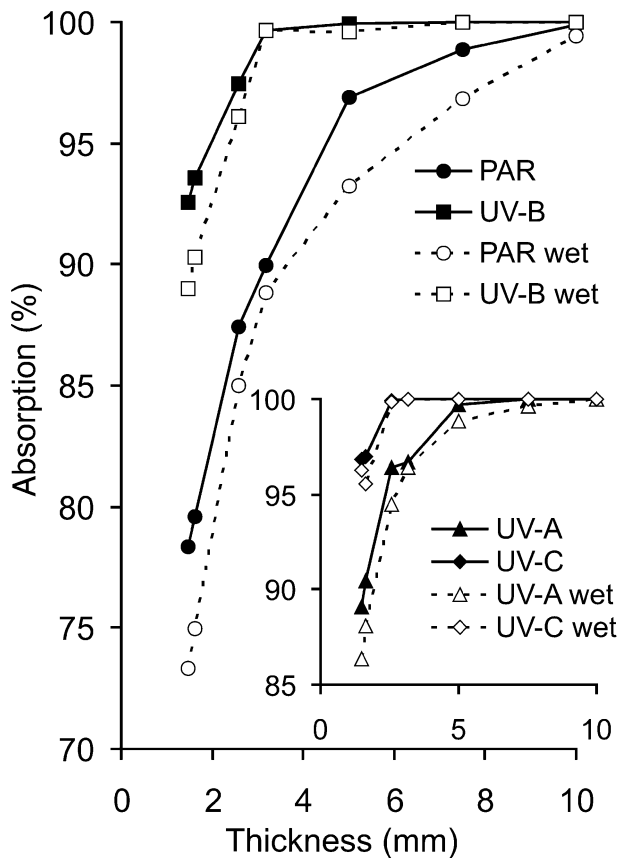


Fig. 7 Comparison of attenuation of PAR, UV-A, UV-B and UV-C by dry and wet wafers of sinter sample a (milky white sinter). Solid lines and solid symbols = dry sinter; dashed lines and clear symbols = wet sinter (i.e. sinter soaked in 5 mM SiO_2 solution).

Ibelings & Maberly, 1998) and thus living below the sinter surface shields the organism from this detrimental effect.

Even so, sufficient PAR must reach the phototrophs at depth to allow them to function. Minimum requirements for photosynthesis are as low as just $5 \mu\text{mol m}^{-2} \text{s}^{-1}$ PAR (Wyman & Fay, 1986; Hu *et al.*, 2000). Figure 8 shows the calculated PAR

intensities at different depths within the three sinter samples for surface intensities of 1000 and $2600 \mu\text{mol m}^{-2} \text{s}^{-1}$ (PAR intensities ranged between these values for 9 h each day during the field study). Considering the minimum PAR intensities required for photosynthesis, it is evident that sufficient PAR penetrates the sinter to approximately 5–10 mm, depending on sinter type (Fig. 8). Thus a favourable niche occurs between ~1 mm, and 5–10 mm where UV and PAR occur at favourable intensities.

Although sinters wetted with 5 mM SiO_2 solution exhibited slightly greater transmittance than dry sinters, the impact of wetting was small (e.g. Fig. 7) and did not have a significant impact on the depth at which favourable light levels occur. For example, wet and dry sinters both reduce maximum midday UV-B to favourable levels ($<1 \text{ Wm}^{-2}$) within ~1 mm of the sinter surface. Wetting the sinter had the largest impact on PAR penetration, although again the impact was relatively small. For example, at an incident PAR intensity of $2600 \mu\text{mol m}^{-2} \text{s}^{-1}$ sinter 'a' at 1.5 mm depth exhibits a PAR irradiance of 563 and $693 \mu\text{mol m}^{-2} \text{s}^{-1}$ when dry and wet, respectively. This is unlikely to cause a big impact on the cyanobacterial community, but could possibly force more PAR sensitive species at most ~0.5 mm deeper into the sinter. Wet sinter could potentially enable the minimum depth for photosynthesis to occur deeper into the rock. For example, the inset of Fig. 8 compares PAR irradiance between wet and dry sinter 'a'. By extrapolation, it appears that deeper PAR penetration in the wet sinter may allow photosynthesis ~2 mm deeper than in the dry sample. It should be noted that this is the most extreme example, and increases in PAR penetration due to wetting are less for the other sinters. The depths of UV attenuation and PAR transmission, in both wet and dry sinters, are consistent with the depth at which viable cyanobacterial communities were found within the sinter.

Occasionally, we also found cryptoendolithic cyanobacteria even deeper at 15 mm below the sinter surface. In these cases it appeared to be due to the presence of larger pore cavities in these zones enabling deeper PAR transmission. Our

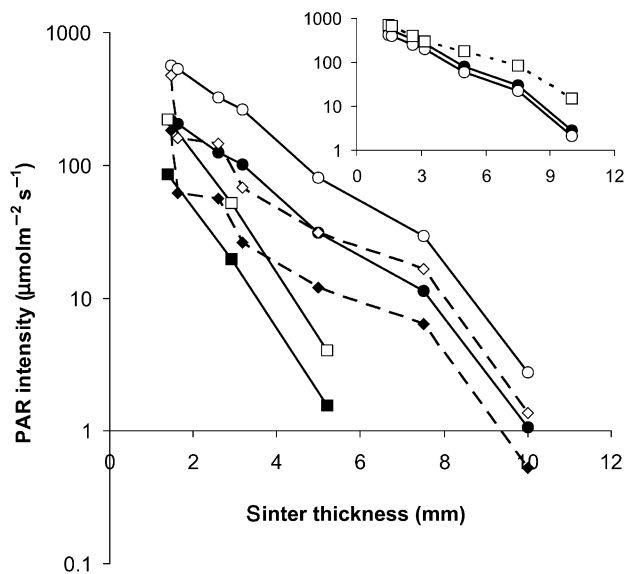


Fig. 8 Calculated PAR intensities at different depths within the three sinter samples for surface intensities of 1000 (solid symbols) and 2600 (clear symbols) $\mu\text{mol m}^{-2} \text{s}^{-1}$. Circles (sinter sample a: milky white sinter dominated by clear opal), diamonds (sinter sample b: grey sinter dominated by less translucent inclusion rich opal), squares (sinter samples c: sinter composed of cemented silica ooides). **Inset:** PAR penetration into sinter sample 'a'. At an incident intensity of 2600 $\mu\text{mol m}^{-2} \text{s}^{-1}$ representative of present day maximum PAR (black circles). The effect of 'wet' sinter on PAR penetration (clear squares). PAR penetration by a 25% less luminous Archean Sun (clear circles).

observations are consistent with similar studies of light transmission in other materials and reports of cryptoendolithic phototrophs at extremely low light levels in limestone and sandstone (e.g. Nienow *et al.*, 1988; Matthes *et al.*, 2001).

Whilst the radiometers used in this study have proved effective in evaluating light attenuation, it would be useful to further investigate the microscale scattering optics within these systems. Evaluation of microscale scattering optics has been achieved in the past by inserting ultrafine fibre-optic radiance and scalar irradiance microprobes into soft sediments and biofilms (e.g. Kuhl & Jorgensen, 1994; Garcia-Pichel & Bebout, 1996). Such an approach allows evaluation of the directional properties of the scattered light field and the integration of light from all directions incident upon a point (the scalar irradiance). This approach is pertinent for future studies of silicified biofilms, although whether the use of fibre-optic probes is possible in solid sinter remains to be seen (the probe could not simply be pushed into the sinter; instead a $\sim 100\text{-}\mu\text{m}$ diameter hole would have to be drilled, which could be problematic in friable sinter). Photons passing through the sinter or biofilm are either absorbed or scattered upon impact with each particle. Evaluating the way the light field is controlled by these two processes can enhance our understanding of how the sinter or biofilm attenuates light. For example, although photon scattering is an important component of light attenuation, in some cases scattering can actually increase irradiance.

This phenomenon, known as light trapping, commonly happens within the upper millimetre of sediments and biofilms (e.g. Kuhl & Jorgensen, 1994; Garcia-Pichel & Bebout, 1996). This happens when incident directional light enters the scattering media and is scattered but not lost from the system. For example, a given point will receive downwelling photons and additional upwelling photons backscattered by particles below (Kuhl & Jorgensen, 1994). Ultimately, organisms within these zones will be exposed to greater irradiance than that incident at the surface (Kuhl & Jorgensen, 1994; Garcia-Pichel & Bebout, 1996). Due to the friability of our sinter, we were unable to determine the photon attenuation properties of the upper millimetre; however, such near-surface trapped light zones are likely present within these sinters, exacerbating the already high levels of solar radiation there and making these zones even more unfavourable for cyanobacteria.

Due to experimental design, backscattered upwelling photons were not measured, and thus the values reported here are not of full scalar irradiance. Measuring scalar irradiance would allow fine tuning of the attenuation profile and enable better understanding of the microscale scattering optics of the sinters. Measurements on siliceous sediments have shown that the upwelling component of the light field (below the light trapping zone) can contribute around 20% of the total scalar irradiance at a given point within the sediment (Kuhl & Jorgensen, 1994). Whilst a contribution as much as 20% from upwelling photons to the scalar irradiance would have only a very minor impact on the light attenuation profiles and cyanobacterial refuge depths reported here (the impact being smaller than the effects of wetting as shown in Fig. 7 and discussed above), these parameters should be determined to enhance our model.

The observation that UV-A is transmitted by the sinter to a greater extent than UV-B may be beneficial to cryptoendolithic organisms, as UV-B damage can be counteracted by UV-A (Quesada *et al.*, 1995). The physiological mechanisms behind this process are unclear, but may involve production of shock proteins that protect against photoinhibition, or promotion of a gene that encodes for the photosystem II reaction centre protein D1 (Shuster *et al.*, 1988; Shibata *et al.*, 1991; Christopher & Mullet, 1994; Quesada *et al.*, 1995). UV-B damage may also be counteracted by blue light (Hirotsawa, 1984; Eker *et al.*, 1990; Han *et al.*, 2001). Possibly, the greater transmission of PAR compared to UV-B through sinter may enable blue light-activated photorepair mechanisms.

The surface mat communities found in the geyser discharge aprons are exposed to the greatest levels of solar radiation because hydrous amorphous silica encrustation is much thinner and water depths are insufficient to afford any attenuation of UV-B. For these surface communities, mechanisms such as phototaxis, matting habit, pigmentation and photorepair mechanisms are fundamental to mat survival (e.g. Garcia-Pichel & Castenholz, 1991; Quesada & Vincent, 1997; Dillon & Castenholz, 1999; Nadeau *et al.*, 1999).

However, our data suggest that even the very thin amorphous silica layers, precipitated in only a few hours or days on these cyanobacterial filaments, act as an additional UV shield (Fig. 5). Considering that cyanobacteria were encrusted by up to 5- μm -thick of hydrous amorphous silica, each individual filament would have its own siliceous UV screen and therefore the cumulative UV attenuation capacity of each encrusted filament stacked one upon another in a mat would significantly reduce the depth to which detrimental UV intensities could penetrate. For the phototrophs within the surface biofilms one must also consider the interactions between oxygen and UV radiation. In environments where O_2 concentrations are high, the production of oxidative radicals by UV radiation can exacerbate the direct impacts of UV radiation, particularly the detrimental effects of UV-A (Jagger, 1985; Garcia-Pichel, 1998). This is commonly problematic in surface biofilms where oxygen levels likely reach supersaturation, particularly in the near surface where light trapping increases irradiance. (Garcia-Pichel, 1998). However, this is less likely to be a problem for cryptoendoliths and sub surface layers in stromatolites where lower PAR levels and lower cell numbers likely aid in restricting O_2 production. This, combined with strong UV attenuation in these environments is bound to minimize this exacerbating effect.

The difference in community composition between the surface biofilms and stromatolites and those in the cryptoendolithic communities indicates each genera is inhabiting a preferred niche. *Lyngbya* spp. dominates in the surface biofilms yet is absent from the cryptoendolithic communities; possibly this genera is most suited to the extremes of solar radiation incident at the sinter surface. In contrast, *Chroococcidiopsis* spp. was only found in the cryptoendolithic communities, apparently preferring the highly protective environment within the sinter. Interestingly, *Phormidium* spp. is able to inhabit all three niches, possibly protected in the biofilm by the UV resistant species *Lyngbya* spp.

Implications for early Precambrian photosynthetic communities

During the Archean and early Proterozoic, photosynthetic life was exposed to considerably higher levels of UV-B than the levels that reach the Earth's surface today. Cockell (2000) estimates Archean UV-B flux at sea level at a solar zenith angle of 0° was five times greater than today, and micro-organisms living at that time would have been exposed to highly detrimental levels of UV-C radiation. UV-C is considerably more damaging than UV-B, perhaps reaching the Earth's surface in the most damaging range of 240–270 nm at intensities as high as 1–3 W m^{-2} (Pierson *et al.*, 1993) (no UV-C reaches the Earth's surface today primarily due to the presence of stratospheric ozone). Shallow marine communities, especially those intermittently exposed to the atmosphere, would have required effective UV-screening mechanisms to survive catastrophic UV levels, while still having access to sufficient PAR for photosynthesis.

Due to the high concentration of dissolved silica and concomitant widespread precipitation of amorphous silica in the ancient oceans (Holland, 1984; Siever, 1992; Sugitani, 1992), Precambrian photosynthetic life likely developed in a habitat where silica precipitation was occurring, similar to that experienced by the cyanobacteria in the discharge aprons at El Tatio geysers. This hypothesis is supported by the occurrence of Archean and early Proterozoic silicified microbes, cherts and siliceous stromatolites composed of primary silica (e.g. Cloud, 1965; Lowe, 1983; Sugitani, 1992). For example, Cloud (1965), while examining fossilized microflora from stromatolites of the Gunflint formation (~2.0 Ga) reported that primary silica appeared to have enveloped the organisms 'at the time of growth, or shortly after . . . probably as a tough gelatinous mass'. Our studies suggest that cell encrustation by hydrous amorphous silica would have afforded organisms with a significant shield against UV radiation, particularly against UV-C, while still allowing significant transmission of PAR (Fig. 5). This is corroborated by previous laboratory based studies where cyanobacteria encrusted in amorphous silica, ~5 μm thick, exhibited dramatically greater resistance to UV-C compared to nonsilicified cyanobacteria (Phoenix *et al.*, 2001). Furthermore, the silica encrustation would have worked in concert with active UV screening mechanisms, such as matting habit (Rambler & Margulis, 1980), pigmentation (Garcia-Pichel & Castenholz, 1991; Dillon & Castenholz, 1999), phototaxis (Margulis *et al.*, 1976) and photorepair mechanisms (Walter, 1983), to enhance the UV resistance of a microbial mat or biofilm. Encrustation would have enabled microbes to spend less energy on implementing and maintaining the active mechanisms.

An important issue to this study, however, is the nature of the adaptations to silica encrustation, and the mechanisms that allow cyanobacteria to continue to function when encrusted in several microns of amorphous silica. Phoenix *et al.* (2000) demonstrated that a cyanobacteria's extracellular sheath appears to act as a barrier to the colloidal silica, restricting silica accumulation to the outer surface of the sheath and preventing silicification of the more sensitive cell wall and cytoplasm. Furthermore, silicification did not inhibit rates of photosynthesis (Phoenix *et al.*, 2000, 2001), and by inference, the permeation of gases essential for photosynthetic productivity. From our TEM results, silica colloids are clearly restricted to the outer surface of the sheath, with no silicification of the cell wall or cytoplasm (Fig. 3). It is possible therefore that one of the functions of the sheath of early Precambrian cyanobacteria was to enable the micro-organism to function in an environment subjected to extensive mineral precipitation.

This current study corroborates previous work by Pierson *et al.* (1993), who demonstrated that habitation of rocks and sediment would provide an effective niche against UV radiation in the Early Precambrian. Photosynthetic microbes living within the shallow water silica stromatolites would also have been efficiently protected from UV. As shown in Fig. 6, the

most harmful waveband, UV-C, is reduced to zero within 1–2.5 mm of the sinter surface. UV-B radiation is also efficiently attenuated; even UV-B levels five times greater than today would be reduced to tolerable near zero levels within 1–2.5 mm of the sinter surface. Archean phototrophs living below these depths would have been well shielded from UV by the sinter. These organisms would also have received sufficient PAR for photosynthesis. Taking into account a 25% less luminous Sun during the Archean (Gough, 1981) has little impact on the depth of PAR penetration (Fig. 8, inset). Thus again sufficient PAR was able to penetrate to between 5 and 10 mm, creating a highly protective niche approximately 4–7 mm thick where UV is favourably attenuated and PAR is sufficiently transmitted. Phototrophs would also have found protective niches by forming cryptoendolithic communities in old aerially exposed stromatolite mounds. Of course, the microbes inhabiting surface biofilms and silica stromatolites of the Precambrian oceans could not have prevented their entombment and burial within silica. It is simply fortuitous then, that they inhabited a silicifying environment which afforded them protection from solar radiation. This contrasts with the cryptoendolithic communities that would choose to inhabit the sinter at depth, driven there, in particular, by high levels of incident solar radiation.

CONCLUSION

This study examines a unique field site where the precipitation of hydrous amorphous silica affords cyanobacteria with an effective screen against UV radiation. El Tatio may represent a reasonable analogue of early Precambrian subaerial, and shallow marine environments undergoing intense exposure to solar UV radiation. Archean and early Proterozoic cyanobacteria in the period before the increase in atmospheric O₂ produced an effective O₃ shield, may have been protected either by becoming passively encrusted by hydrous amorphous silica or by inhabiting siliceous structures such as cryptoendoliths and stromatolites. The characteristic property of the hydrous amorphous silica precipitates and sinter deposits at El Tatio effectively attenuate UV-B and UV-C while transmitting sufficient PAR for photosynthesis. The role of silica, in its ability to create effective UV screened habitats for phototrophs, is fundamental to the adaptation and evolution of life in extreme habitats today and in the past.

ACKNOWLEDGEMENTS

We thank Kitty Milliken and John Lansdown for analytical support, and Suzanne Pierce for analytical and logistical support. This work was supported by a National Science Foundation award (EAR0085576) to PCB, and Natural Science and Engineering Research Council (NSERC) of Canada and Ontario Premier's Research Excellence awards to FGF. Travel to Chile was supported in part by the Geology Foundation of the Jackson School of Geosciences.

REFERENCES

- Awramik SM, Schopf JW, Walter MR (1983) Filamentous fossil bacteria from the Archean of Western Australia. *Precambrian Research* **20**, 357–374.
- Berkner LV, Marshall LC (1965) On the origin and rise of oxygen concentration in the Earth's atmosphere. *Journal of Atmospheric Science* **22**, 225–261.
- Cady SL, Farmer JD (1996) Fossilization processes in siliceous thermal springs: trends in preservation along thermal gradients. In *Evolution of Hydrothermal Ecosystems on Earth (and Mars?)* (eds Brock GR, Goode JA). Wiley, Chichester, pp. 150–173.
- Caldwell MM, Teramura AH, Tevini M (1989) The changing solar ultraviolet climate and the ecological consequences for higher plants. *Tree* **4**, 363–367.
- Christopher DA, Mullet JE (1994) Separate Photosensory pathways co-regulate blue-light/ultraviolet-A-activated psbD-psbC transcription and light-induced D2 and CP43 degradation in barley (*Hordeum vulgare*) chloroplasts. *Plant Physiology* **104**, 1119–1129.
- Cloud PE Jr (1965) Significance of the Gunflint (Precambrian) microflora. *Science* **148**, 27–35.
- Cockell CS (2000) Ultraviolet radiation and the photobiology of the Earth's early oceans. *Origins of Life and Evolution of the Biosphere* **30**, 467–499.
- Cockell CS (2002) Photobiological uncertainties in the Archean and post-Archean world. *International Journal of Astrobiology* **1**, 31–38.
- Dillon JG, Castenholz RW (1999) Scytonemin, a cyanobacterial sheath pigment, protects against UVC radiation: implications for early photosynthetic life. *Journal of Phycology* **35**, 673–681.
- Dillon JG, Miller SR, Castenholz RW (2003) UV-acclimation responses in natural populations of cyanobacteria (*Calothrix* sp.). *Environmental Microbiology* **5**, 473–483.
- Donkor V, Hader D-P (1991) Effects of solar and ultraviolet radiation on motility, photomovement and pigmentation in filamentous, gliding cyanobacteria. *FEMS Microbiology Ecology* **86**, 159–168.
- Dunlop JSR, Muir MD, Milne VA, Groves DI (1978) A new microfossil assemblage from the Archean of Western Australia. *Nature* **274**, 676–678.
- Eker AP, Kooiman P, Hessels JKC, Yasui A (1990) DNA photoreactivating enzyme from the cyanobacterium *Anacystis nidulans*. *Journal of Biological Chemistry* **14**, 8009–8015.
- El Tabakh M, Grey K, Pirajno F, Schreiber BC (1998) Pseudomorphs after evaporitic minerals interbedded with 2.2 Ga stromatolites of the Yerrida basin, Western Australia: origin and significance. *Geology* **27**, 871–874.
- Fernandez-Turiel JL, Garcia-Valles M, Gimeno-Torrente D, Saavedra-Alonso J, Martinez-Manent S (2005) The hot spring and geyser sinters of El Tatio, northern Chile. *Sedimentary Geology* **180**, 125–147.
- Fournier RO, Potter RW II (1982) A revised and expanded silica (quartz) geothermometer. *Geothermal Resources Council Bulletin* **11**, 3–12.
- Garcia-Pichel F (1998) Solar ultraviolet and the evolutionary history of cyanobacteria. *Origins of Life and Evolution of the Biosphere* **28**, 321–347.
- Garcia-Pichel F, Castenholz RW (1991) Characterization and biological implications of scytonemin, a cyanobacterial sheath pigment. *Journal of Phycology* **27**, 395–409.
- Garcia-Pichel F, Bebout BM (1996) Penetration and ultraviolet radiation into shallow water sediments: high exposure for photosynthetic communities. *Marine Ecology Progress Series* **131**, 257–262.

- Giggenbach WF (1978) The isotopic composition of waters from the El Tatio geothermal field, Northern Chile. *Geochimica et Cosmochimica Acta* **42**, 979–988.
- Glennon JA, Pfaff RM (2003) The extraordinary thermal activity of El Tatio Geyser Field, Antofagasta Region, Chile. *Geyser Observation and Study Association (GOSA) Transactions* **8**, pp. 31–78.
- Gough DO (1981) Solar interior structure and luminosity variations. *Solar Physics* **74**, 21–34.
- Hader D-P, Watanabe M, Fuyura M (1986) Inhibition of motility in the cyanobacterium, *Phormidium uncinatum*, by solar and monochromatic UV irradiation. *Plant Cell Physiology* **27**, 887–894.
- Hader D-P, Worrest RC (1991) Effects of enhanced solar ultraviolet radiation on aquatic ecosystems. *Photochemistry and Photobiology* **53**, 717–725.
- Han T, Sinha RP, Hader D-P (2001) UV-A/blue light-induced reactivation of photosynthesis in UV-B irradiated cyanobacterium, *Anabaena* sp. *Journal of Plant Physiology* **158**, 1403–1413.
- Hirosawa T (1984) Near UV and blue light effects on cyanobacteria. In *Blue Light Effects in Biology Systems* (ed. Senger H). Springer-Verlag, Berlin, pp. 39–47.
- Hofmann HJ, Grey K, Hickman AH, Thorpe RI (1999) Origin of 3.45 Ga coniform stromatolites in Warrawoona Group, Western Australia. *Geological Society of America Bulletin* **111**, 1256–1262.
- Holland HD (1984) *The Chemical Evolution of the Atmosphere and Oceans*. Princeton University Press, Princeton, New Jersey.
- Hu Q, Westerhoff P, Vermass W (2000) Removal of nitrate from groundwater by cyanobacteria: quantitative assessment of factors influencing nitrate uptake. *Applied and Environmental Microbiology* **66**, 133–139.
- Ibelings BW, Maberly SC (1998) Photoinhibition and the availability of inorganic carbon restrict photosynthesis by surface blooms of cyanobacteria. *Limnology and Oceanography* **43**, 408–419.
- Iler RK (1979) *Chemistry of Silica: Solubility, Polymerization, Colloid and Surface Properties and Biochemistry*. Wiley Interscience, New York.
- Jagger J (1985) *Solar-UV Actions on Living Cells*. Praeger, New York.
- Jeffery WH, Aas P, Lyons MM, Coffin RB, Ralph JP, Mitchell DL (1996) Ambient solar radiation-induced photodamage in marine bacterioplankton. *Photochemistry and Photobiology* **64**, 419–427.
- Jones B, Renault RW, Rosen MR (1998) Microbial biofacies in hot-spring sinters: a model based on Ohaaki Pool, North Island, New Zealand. *Journal of Sedimentary Research* **68**, 413–434.
- Jones B, Renault R (1997) Formation of silica oncoids around geysers and hot springs at El Tatio, northern Chile. *Sedimentology* **44**, 287–304.
- Kasting JF (1987) Theoretical constraints on oxygen and carbon dioxide concentrations in the Precambrian atmosphere. *Precambrian Research* **34**, 205–229.
- Konhauser KO, Phoenix VR, Adams DG, Bottrell SH, Head IM (2001) Microbial–silica interactions in modern hot spring sinter: possible analogues for some Precambrian siliceous stromatolites. *Sedimentology* **48**, 415–433.
- Kuhl M, Jorgensen BB (1994) The light field of microbenthic communities: Radiance distribution and microscale optics of sandy coastal sediments. *Limnology and Oceanography* **39**, 1368–1398.
- Lahsen A, Trujillo P (1976) El Tatio geothermal field. In *Proceedings of the 2nd United Nations Symposium on Geothermal Fields*. Berkeley, CA, pp. 157–178.
- Litchman E (2000) Growth rates of phytoplankton under fluctuating light. *Freshwater Biology* **44**, 233–235.
- Litchman E, Steiner D, Bossard P (2003) Photosynthetic and growth responses of three freshwater algae to phosphorous limitation and daylength. *Freshwater Biology* **48**, 2141–2148.
- Lowe DR (1980) Stromatolites 3400-Myr old from the Archean of Western Australia. *Nature* **284**, 441–443.
- Lowe DR (1983) Restricted shallow-water sedimentation of early Archean stromatolitic and evaporitic strata of the Strelley Pool Chert, Pilbara Block, Western Australia. *Precambrian Research* **19**, 239–283.
- Mahon WAJ (1971) Survey for geothermal development in Northern Chile: the geochemistry of the fluids discharged from hole 5 El Tatio geothermal system. *United Nations Development Program*, New York, NY, USA.
- Margulis L, Walker JGC, Rambler M (1976) Reassessment of roles of oxygen and ultraviolet light in Precambrian evolution. *Nature* **264**, 620–624.
- Matthes U, Turner SJ, Larson DW (2001) Light attenuation by limestone rock and its constraint on the depth distribution of endolithic algae and cyanobacteria. *International Journal of Plant Science* **162**, 263–270.
- McCleskey RB, Nordstrom DK, Maest AS (2004) Preservation of water samples for arsenic (III/V) determinations: an evaluation of the literature and new analytical results. *Applied Geochemistry* **19**, 995–1009.
- Miller SR, Wingard CE, Castenholz RW (1998) Effects of visible light and UV radiation on photosynthesis in a population of a hot spring cyanobacterium, a *Synechococcus* sp., subjected to high-temperature stress. *Applied and Environmental Microbiology* **64**, 3893–3899.
- Nadeau TL, Howard-Williams C, Castenholz RW (1999) Effects of solar UV and visible irradiance on photosynthesis and vertical migration of *Oscillatoria* sp. (cyanobacteria) in an Antarctic microbial mat. *Aquatic Microbial Ecology* **20**, 231–243.
- Nienow JA, McKay CP, Friedmann EI (1988) The cryptoendolith microbial environment in the Ross Desert of Antarctica: light in the photosynthetically active region. *Microbial Ecology* **16**, 271–289.
- Olson JM (1981) Evolution of photosynthetic reaction centres. *Biosystems* **14**, 89–94.
- Paelr HW, Bland PT, Bowles D, Haibach ME (1985) Adaption to high intensity, low wavelength light among surface blooms of the cyanobacterium *Micocystis aruginosa*. *Applied and Environmental Microbiology* **49**, 1046–1052.
- Parkhurst DL, Appelo CAJ (1999) *A User's Guide to PHREEQC (Version 2) – A Computer Program for Speciation, Batch-Reaction, One-Dimensional Transport, and Inverse Geochemical Calculations*. Water-Resources Investigations Report 99-4259. US Geological Survey, Denver.
- Phoenix VR, Adams DG, Konhauser KO (2000) Cyanobacterial viability during hydrothermal biomineralisation. *Chemical Geology* **169**, 329–338.
- Phoenix VR, Konhauser KO, Adams DG, Bottrell SH (2001) Role of biomineralization as an ultraviolet shield: implications for Archean life. *Geology* **29**, 823–826.
- Piazena H (1996) The effect of altitude upon the solar UV-B and UV-A irradiance in the tropical Chilean Andes. *Solar Energy* **57**, 133–140.
- Pierson BK, Mitchell HK, Ruff-Roberts AL (1993) *Chloroflexus aurantiacus* and ultraviolet radiation: implications for Archean shallow-water stromatolites. *Origins of Life and Evolution of the Biosphere* **23**, 243–260.
- Quesada A, Mouget J-L, Warwick FV (1995) Growth of Antarctic cyanobacteria under ultraviolet radiation: UVA counteracts UVB inhibition. *Journal of Phycology* **31**, 242–248.
- Quesada A, Vincent WF (1997) Strategies of adaptation by Antarctic cyanobacteria to ultraviolet radiation. *European Journal of Phycology* **32**, 335–342.
- Rambler MB, Margulis L (1980) Bacterial resistance to ultraviolet irradiation under anaerobiosis: implications for pre-Phanerozoic evolution. *Science* **210**, 638–640.

- Rippka R, Deruelles J, Waterbury JB, Herdman M, Stanier RY (1979) Generic assignments, strain histories and properties of pure cultures of cyanobacteria. *Journal of General Microbiology* **111**, 1–61.
- Sagan C (1973) Ultraviolet selection pressure on the earliest organisms. *Journal of Theoretical Biology* **39**, 195–200.
- Schultze-Lam S, Ferris FG, Konhauser KO, Wiese RG (1995) In-situ silicification of an Icelandic hot spring microbial mat: implications for microfossil formation. *Canadian Journal of Earth Sciences* **32**, 2021–2026.
- Shibata H, Baba K, Ochiai H (1991) Near UV irradiation induces shock proteins in *Anacystis nidulans* R-2; possible role of active oxygen. *Plant Cell Physiology* **32**, 771–776.
- Shuster G, Even D, Loppstech K, Ohad I (1988) Evidence for protection by heat-shock proteins against photoinhibition during heat shock. *EMBO Journal* **7**, 1–6.
- Siever R (1992) The silica cycle in the Precambrian. *Geochimica et Cosmochimica Acta* **56**, 3265–3272.
- de Silva SL, Francis PW (1991) *Volcanoes of the Central Andes*. Springer, Berlin.
- Sugitani K (1992) Geochemical characteristics of Archean cherts and other sedimentary rocks in the Pilbara Block, Western Australia: evidence for Archean seawater enriched in hydrothermally-derived iron and silica. *Precambrian Research* **57**, 21–47.
- Tevini M (1993) Molecular biological effects of ultraviolet radiation. In *UV-B radiation and ozone depletion: effects on humans, animals, plants microorganisms and materials* (ed. Tevini M). Lewis, Boca Raton, Florida, pp. 1–16.
- Walker JGC, Klein C, Schidlowski M, Schopf JW, Stevenson DJ, Walter MR (1983) Environmental evolution of the Archean-early Proterozoic Earth. In *Earth's Earliest Biosphere* (ed. Schopf JW). Princeton University Press, New Jersey, Princeton, pp. 261–290.
- Walsby AE (1968) Mucilage secretion and the movements of blue-green algae. *Protoplasma* **65**, 223–238.
- Walter MR (1972) A hot spring analog for the depositional environment of Precambrian iron formations of the Lake Superior Region. *Economic Geology* **67**, 965–980.
- Walter MR (1983) Archean stromatolites: evidence of the Earth's earliest benthos. In *Earth's Earliest Biosphere* (ed. Schopf WJ). Princeton University Press, Princeton, New Jersey, pp. 187–213.
- Wyman M, Fay P (1986) Underwater light climate and the growth of pigmentation of planktonic blue-green algae (Cyanobacteria) I. The influence of light quantity. *Proceedings of the Royal Society of London. Series B-Biological Sciences* **227B**, 367–380.